Int. J. Heat Mass Transfer. Vol. 33, No. 2, pp. 287–299, 1990
Printed in Great Britain

0017–9310/90 $3.00 + 0.00
© 1990 Pergamon Press plc

Transient binary mixture natural convection in square enclosures

T. F. LIN, C. C. HUANG and T. S. CHANG
Department of Mechanical Engineering, National Chiao Tung University, Hsinchu, Taiwan, R.O.C.

(*Received* 11 *November* 1987 *and in final form* 9 *May* 1989)

Abstract—A detailed numerical study has been carried out to investigate transient natural convection in a binary mixture in square enclosures with the simultaneous presence of temperature and concentration gradients. Results are particularly presented to illustrate the effects of the combined thermal and solutal buoyancy forces on the temporal evolution of the flow pattern and the associated heat and mass transfer for both augmenting and opposing flows. The effects of the buoyancy ratio are found to be rather significant on the flow pattern and heat and mass transfer especially for the opposing flows.

1. INTRODUCTION

NATURAL convective flows occurring in the natural environment and technological processes are often driven by the combined buoyancy forces of heat and mass transfer. Transfer processes across the ocean–air interface, control of human body temperature through simultaneous diffusion of the metabolic heat and perspiration, evaporative cooling of high temperature systems, and crystal growth from the fluid phase are just a few examples where the combined buoyancy effects exhibit profound influences. Although natural convection resulting from thermal buoyancy alone has been extensively studied in the past, natural convection due to the combined buoyancy forces has not received enough attention.

Early studies [1–6] on the natural convection heat and mass transfer primarily focused on the flow over a long vertical surface in which the two buoyancy forces act in the same or opposite directions. For this simple geometry the flows are normally of boundary layer type. A critical review on natural convection with combined driving forces given by Ostrach [7] pointed out that various modes of flow are possible depending on the orientation of the buoyancy forces. Multicomponent natural convection in cavities in relation to the processes of crystal growth has received increased attention. The importance of the transport processes in conjunction with the crystal growth by various growth methods was indicated by Ostrach [8]. Up-to-date reviews on the buoyancy effects in the processes of crystal growth from a melt were presented by Pimputkar and Ostrach [9] and by Langlois [10]. A similar review on the combined buoyancy effects in crystal growth from vapours was conducted by Rosenberger [11]. Recently, Rosenberger and his co-workers [12, 13] showed profound multicomponent effects during the crystal growth from the chemical vapour deposition in closed ampoules.

More recently, laboratory experiments were conducted to observe the cell patterns in thermosolutal convection flows in shallow enclosures by Kamotani *et al.* [14], Ostrach *et al.* [15], Lee and Hyun [16] and Wang and Chuang [17]. In these studies both augmenting and opposing horizontal temperature and concentration gradients were considered. Under different experimental conditions various complex flow patterns were noted; furthermore, the flow can become unsteady under certain conditions. In contrast to the above studies [14–17], Ranganathan and Viskanta [18] performed numerical calculations to study the steady features of flow, and the associated heat and mass transfer for binary gas natural convection in rectangular cavities relevant to chemical vapour deposition processes. A similar study has been conducted by Trevisan and Bejan [19] by using analytical and numerical techniques to investigate flow, heat and mass transfer phenomena under various conditions. Scale analysis of the problem for the extreme cases of heat transfer-driven or mass transfer-driven situations in the boundary layer flow regime covering wide ranges of Prandtl and Schmidt numbers were carried out by Bejan [20], which complemented the old analyses [1–6]. Close scrutiny on the literature just reviewed [12–20] reveals that the cell patterns and the characteristics of heat and mass transfer in the flows are substantially influenced by all the governing parameters: the Prandtl number, Schmidt number, aspect ratio, ratio of the buoyancy forces, and Grashof number. However, details of the transport processes in the flows are still not fully understood.

To explore the detailed mechanisms of momentum, energy, and species transfer in the thermosolutal convection, time-accurate solutions for the governing differential equations are required. As a preliminary attempt to improve our understanding on the natural convection resulting from the combined driving forces, the present study investigates unsteady binary mixture natural convection in square enclosures resulting from the simultaneous presence of horizontal temperature and concentration gradients by numerically solving the problem with the SIMPLER

NOMENCLATURE

D binary mass diffusion coefficient
g gravitational acceleration
Gr Grashof number for heat transfer, equation (6)
L height and width of enclosure
Le Lewis number, Sc/Pr
N buoyancy ratio, equation (6)
Nu_x local Nusselt number, equation (14)
$\overline{Nu}$ average Nusselt number, equation (15)
P dimensionless pressure, equation (6)
p_d dynamic pressure
Pr Prandtl number, ν/α
Sc Schmidt number, ν/D
Sh_x local Sherwood number, equation (14)
$\overline{Sh}$ average Sherwood number
t time
T_C, T_H cold wall and hot wall temperatures
t_R reference time scale, equation (6)
u, v horizontal and vertical velocity components
U, V dimensionless horizontal and vertical velocity components, equation (6)
u_R reference velocity, equation (7)
W dimensionless mass fraction of species 1, equation (6)
w_1 mass fraction of species 1
w_{1H}, w_{1L} high and low mass fractions of species 1
x, y horizontal and vertical coordinates
X, Y dimensionless horizontal and vertical coordinates, equation (6).

Greek symbols
α thermal diffusivity of the mixture
β_M coefficient of volumetric expansion due to concentration change
β_T coefficient of volumetric expansion due to temperature change
θ dimensionless temperature, equation (6)
ν kinematic viscosity of the mixture
ρ mass density of the mixture
τ dimensionless time, equation (6).

Subscripts
L at the left-hand wall
R at the right-hand wall or reference quantity.

algorithm [21–23]. Particular attention is paid to the cell formation from the initial stationary state to the final steady state and the associated temperature and concentration fields under various conditions. Results are specifically reported for the mixture with Prandtl and Schmidt numbers of the order of unity ($Pr = 0.7$ and $Sc = 0.6$), which are pertinent to the chemical vapour transport processes [12, 13].

In the following section the mathematical formulation for the problem is first given. The numerical scheme employed, the grid system and the solution procedures are described in Section 3. Finally, the results from the numerical computations are discussed in detail in Section 4.

2. MATHEMATICAL FORMULATION

Under consideration is a binary fluid contained in a two-dimensional square enclosure. The top and bottom boundaries of the enclosure are thermally well insulated and impermeable. Initially, the stationary fluid and the confining walls are assumed to be at the same uniform temperature T_C and the same uniform concentration w_{1L}. At $t = 0$, the temperature at the left vertical wall is suddenly raised to a higher level T_H and maintained at this level thereafter. Meanwhile, the concentration of the fluid at the left vertical wall or at the right vertical wall, depending on the augmenting or opposing buoyancy forces, is hypothesized to be abruptly elevated to a higher value w_{1H}. Accordingly, horizontal temperature and concentration gradients are imposed on the fluid, and the flow is then initiated and evolves under the action of the combined driving forces due to these gradients. The transient developments of flow, temperature and concentration fields in the cavity can be predicted, with the Boussinesq approximations [7, 13, 18], by solving the following governing differential equations in dimensionless form:

continuity equation

$$\frac{\partial U}{\partial X} + \frac{\partial V}{\partial Y} = 0; \tag{1}$$

x-direction momentum equation

$$\frac{\partial U}{\partial \tau} + U\frac{\partial U}{\partial X} + V\frac{\partial U}{\partial Y} = -\frac{\partial P}{\partial X} + \frac{1}{\sqrt{(Gr)}}\left[\frac{\partial^2 U}{\partial X^2} + \frac{\partial^2 U}{\partial Y^2}\right]; \tag{2}$$

y-direction momentum equation

$$\frac{\partial V}{\partial \tau} + U\frac{\partial V}{\partial X} + V\frac{\partial V}{\partial Y} = -\frac{\partial P}{\partial Y} + \frac{1}{\sqrt{(Gr)}}\left[\frac{\partial^2 V}{\partial X^2} + \frac{\partial^2 V}{\partial Y^2}\right] + (\theta + NW); \tag{3}$$

energy equation

$$\frac{\partial\theta}{\partial\tau}+U\frac{\partial\theta}{\partial X}+V\frac{\partial\theta}{\partial Y}=\frac{1}{Pr\sqrt{(Gr)}}\left[\frac{\partial^2\theta}{\partial X^2}+\frac{\partial^2\theta}{\partial Y^2}\right]; \quad (4)$$

species diffusion equation

$$\frac{\partial W}{\partial\tau}+U\frac{\partial W}{\partial X}+V\frac{\partial W}{\partial Y}=\frac{1}{Sc\sqrt{(Gr)}}\left[\frac{\partial^2 W}{\partial X^2}+\frac{\partial^2 W}{\partial Y^2}\right]. \quad (5)$$

In nondimensionalizing the governing equations, the following dimensionless variables were introduced:

$$U=\frac{u}{u_R},\quad V=\frac{v}{u_R},\quad X=\frac{x}{L},\quad Y=\frac{y}{L}$$

$$P=\frac{p_d}{\rho u_R^2},\quad t_R=\frac{L}{u_R},\quad \tau=\frac{t}{t_R},\quad Pr=\frac{\nu}{\alpha}$$

$$Sc=\frac{\nu}{D},\quad \theta=\frac{T-T_C}{T_H-T_C},\quad W=\frac{w_1-w_{1L}}{w_{1H}-w_{1L}}$$

$$Gr=\beta_T g(T_H-T_C)L^3/\nu^2,\quad N=\frac{\beta_M(w_{1H}-w_{1L})}{\beta_T(T_H-T_C)}$$

$$\Gamma_1=\frac{1-w_{1L}}{w_{1H}-w_{1L}} \quad (6)$$

where

$$u_R=\{\beta_T g(T_H-T_C)L\}^{1/2}. \quad (7)$$

Equations (1)–(5) are subject to the following initial and boundary conditions:

$$\tau\leqslant 0,\quad V=U=P=\theta=W=0 \quad (8)$$

$$Y=0 \text{ and } 1,\quad \partial\theta/\partial Y=\partial W/\partial Y=0. \quad (9)$$

For augmenting cases

$$X=0,\quad \theta=1,\quad W=0,\quad V=0$$

$$U=-\frac{1}{Sc\sqrt{(Gr)}}\frac{1}{\Gamma_1}\frac{\partial W}{\partial X}\bigg|_{X=0} \quad (10)$$

$$X=1,\quad \theta=0,\quad W=1,\quad V=0$$

$$U=-\frac{1}{Sc\sqrt{(Gr)}}\frac{1}{(\Gamma_1-1)}\frac{\partial W}{\partial X}\bigg|_{X=1}. \quad (11)$$

For opposing cases

$$X=0,\quad \theta=W=1,\quad V=0$$

$$U=-\frac{1}{Sc\sqrt{(Gr)}}\frac{1}{(\Gamma_1-1)}\frac{\partial W}{\partial X}\bigg|_{X=0} \quad (12)$$

$$X=1,\quad \theta=W=0,\quad V=0$$

$$U=-\frac{1}{Sc\sqrt{(Gr)}}\frac{1}{\Gamma_1}\frac{\partial W}{\partial X}\bigg|_{X=1}. \quad (13)$$

The interfacial velocities at the vertical walls due to mass transfer, which may be important at early transients, are specified in equations (10)–(13) [24].

It is noticed that the volumetric expansion coefficient due to temperature change, defined as $\beta_T=-(1/\rho)(\partial\rho/\partial T)_{w_1,p}$, is normally positive, but the volumetric expansion coefficient for concentration change, defined as $\beta_M=-(1/\rho)(\partial\rho/\partial w_1)_{T,p}$, can be either positive or negative. In this study β_M is taken to be negative, that is, component 1 is assumed to be heavier than component 2 in the mixture ($\partial\rho/\partial w_1>0$). As a result, the buoyancy ratio N is always negative. To facilitate the analysis, the thermophysical properties of the mixture are considered to be constant except the density in the buoyancy terms [7, 18]. This simplification is appropriate when both components in the mixture have comparable molecular weights or when the mixture is dilute.

Four non-dimensional governing parameters appear in the above formulation, namely, the Prandtl number Pr, Schmidt number Sc, heat transfer Grashof number Gr, and the buoyancy ratio N.

The transient local Nusselt and Sherwood numbers on the vertical walls can be evaluated by

$$Nu_x=\begin{cases}-(\partial\theta/\partial X)_{X=1}, \\ \qquad \text{for the right-hand wall} & (14a)\\ -(\partial\theta/\partial X)_{X=0}, \\ \qquad \text{for the left-hand wall} & (14b)\end{cases}$$

$$Sh_x=\begin{cases}(\partial W/\partial X)_{X=1}, \text{ for the augmenting case at the right-hand wall} & (14c)\\ -(\partial W/\partial X)_{X=1}, \text{ for the opposing case at the right-hand wall} & (14d)\\ (\partial W/\partial X)_{X=0}, \text{ for the augmenting case at the left-hand wall} & (14e)\\ -(\partial W/\partial X)_{X=0}, \text{ for the opposing case at the left-hand wall.} & (14f)\end{cases}$$

Integrating the results for the local Nusselt and Sherwood numbers along a given wall gives the results for the average Nusselt and Sherwood numbers for that wall. For instance, at the right-hand wall

$$\overline{Nu}=\int_0^1[-(\partial\theta/\partial X)_{X=1}]\,dY. \quad (15)$$

3. SOLUTION METHOD

Since the flow governed by equations (1)–(5) is known to be parabolic in time but elliptic in space, the solution for the problem can only be marched in time, and iterative procedures must be employed to obtain the solution in the spatial domain. The SIMPLER (semi-implicit method for pressure-linked revised) algorithm developed by Patankar and Spalding [21–23] was chosen to numerically solve the governing differential equations in their primitive

form. To obtain better convergence properties, the unsteady terms in these equations were implicitly treated and hence approximated by backward differencing. In discretizing the equations in the spatial domain, the X and Y momentum, energy, and species diffusion equations were integrated over the respective control volumes defined on a staggered grid system at the current time level. The pressure and pressure correction equations are derived from the continuity equation to enforce the local mass balance. Consequently, the finite-difference representations for the governing equations became fully implicit.

For each time step the line-by-line method [23] with successive under-relaxation was utilized to solve the finite-difference equations. These equations were alternately swept in the X- and Y-directions until the relative changes between two consecutive iterations in all dependent variables (U, V, θ, and W) at every nodal point was below 10^{-3}. The solutions for the pressure and pressure correction equations were iterated until the local mass balance was achieved to a satisfactory degree. The solutions for the problem were marched from the initial state to the final steady state. Steady state was considered to be attained by three criteria. First of all, the solutions at every node should become almost unchanged with time. In fact, the following criterion:

$$\left|\frac{\phi^{n+1}-\phi^{n}}{\phi^{n+1}}\right| < 10^{-3} \tag{16}$$

was enforced, where ϕ stands for U, V, θ, W, or P. This criterion can sometimes be met when the time interval for the numerical integration of the governing equations is rather small. Other criteria, therefore, were needed. Secondly, we insured that during the steady state the heat input to the fluid through the hot wall must be equal to that leaving the cold wall. This criterion was fulfilled by requiring that

$$\left|\frac{\overline{Nu}_{R}-\overline{Nu}_{L}}{\overline{Nu}_{R}}\right| < 10^{-3}. \tag{17}$$

Finally, the overall mass balance for component 1 at steady state was invoked by checking whether

$$\left|\frac{\overline{Sh}_{R}-\overline{Sh}_{L}}{\overline{Sh}_{R}}\right| < 10^{-3}. \tag{18}$$

During the program tests, 21×21, 31×31, 41×41, 61×61, uniform grid systems were used. The time interval, first set at a relatively small value from 10^{-4} to 10^{-3} depending on Gr and N, is successively enlarged by a factor of 1.005, i.e. $\Delta\tau_n = 1.005\times\Delta\tau_{n-1}$. In the limiting case of no mass transfer in the flow, the predicted flow patterns and temperature fields at the steady state for $Pr = 0.71$ and $Ra = 10^3$–10^6 were in excellent agreement with the benchmark solutions given by de Vahl Davis [25] for the 41×41 grid system. A detailed comparison of the flow and thermal quantities is given in Table 1. To save on computation cost, the results presented are obtained from the 41×41 grid.

4. RESULTS AND DISCUSSION

As was already noted above, the problem under investigation is governed by four non-dimensional groups: the Prandtl number Pr, Schmidt number Sc, Grashof number Gr, and buoyancy ratio N. It is a formidable task to perform computations covering wide ranges of all these parameters. Instead, results were obtained for a given binary gas mixture with Pr and Sc fixed at 0.7 and 0.6, respectively. Besides, Γ_1 is chosen to be 20. Attention is therefore focused herein on the effects of the Grashof number and buoyancy ratio. In presenting results the augmenting and opposing cases need to be separately discussed because the transport processes in these two cases

Table 1. Comparison of Nusselt numbers and flow quantities with benchmark solutions [25] for $Pr = 0.71$, $A = 1$

		$\overline{Nu}$	Nu_{max}	Nu_{min}	U_{max}	V_{max}
$Ra = 10^3$	Benchmark solutions	1.117	1.505	0.692	0.137	0.139
	Present results	1.114	1.497	0.717	0.136	0.149
$Ra = 10^4$	Benchmark solutions	2.238	3.528	0.586	0.192	0.233
	Present results	2.262	3.590	0.587	0.191	0.233
$Ra = 10^5$	Benchmark solutions	4.509	7.717	0.729	0.130	0.257
	Present results	4.655	8.328	0.743	0.131	0.259
$Ra = 10^6$	Benchmark solutions	8.817	17.925	0.989	0.077	0.260
	Present results	8.742	19.360	1.009	0.085	0.267

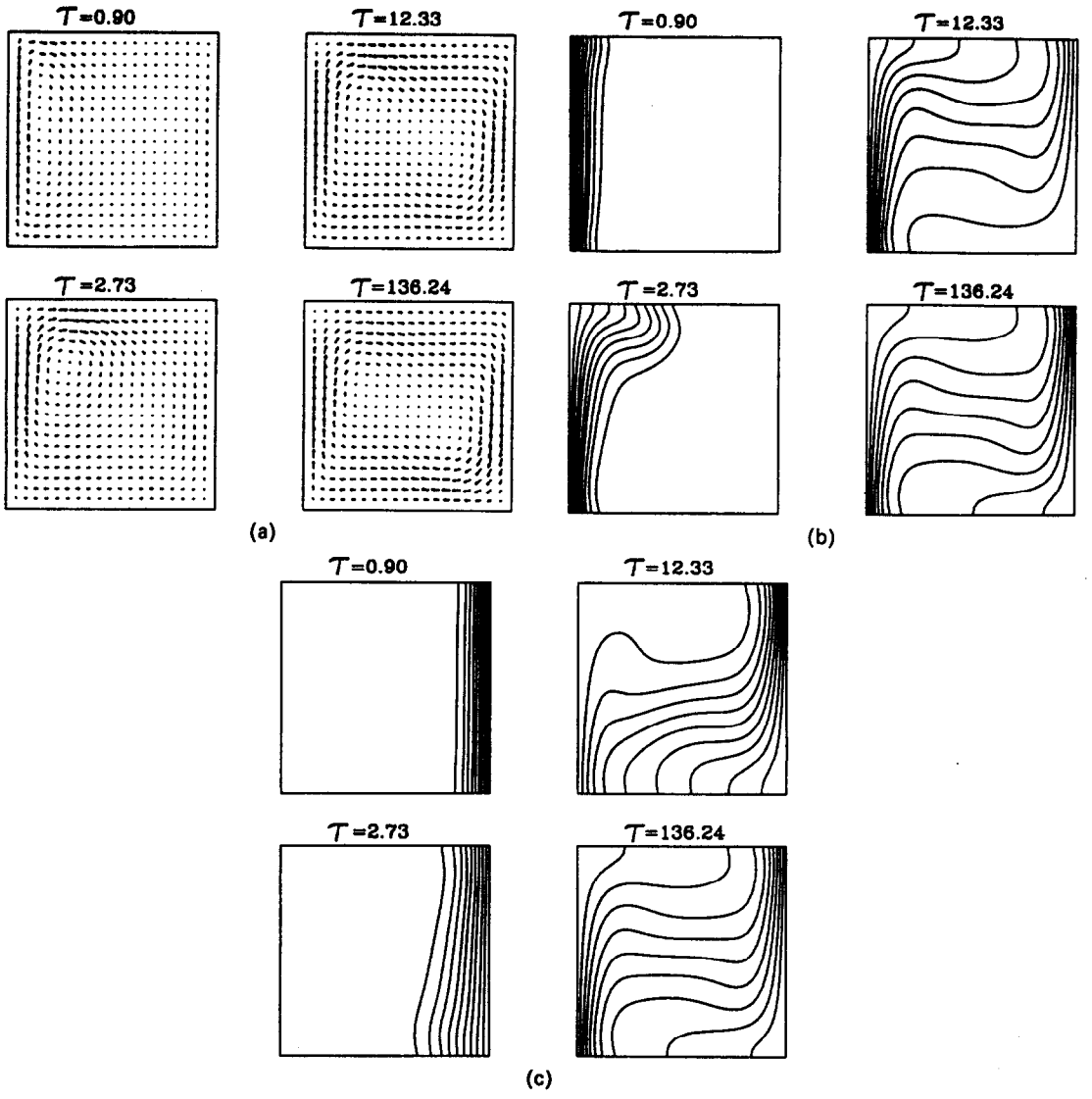

FIG. 1. Time evolution of (a) flow patterns, (b) isotherms and (c) iso-concentration lines in aiding flow for $Gr = 10^5$, $Pr = 0.7$, $Sc = 0.6$, $N = -0.2$.

are rather different. For each case results have been obtained for $Gr = 10^3$–10^6 and $N = -0.2$ to -5.

4.1. *Augmenting flows*

In this case the flow near the hot, left-hand wall is driven vertically upward, and meanwhile the high concentration at the right-hand wall causes the fluid near it to sink. Clearly, both the thermal and solutal buoyancy forces push the fluid clockwise and thus they simultaneously accelerate the flow. The effects of the Grashof number and buoyancy ratio on the temporal developments of the flow, temperature and concentration fields are of particular interest and discussed below.

The transient developments of the fluid flow, temperature and concentration distributions are displayed through vector velocity fields normalized by the maximum value at that time instant and iso-value contours in Figs. 1(a)–(c) for $Gr = 10^5$ and $N = 0.2$. Note that for $N = -0.2$ the driving force from the concentration difference is small compared with that from the temperature difference. The predicted flow patterns shown in Fig. 1(a) need detailed discussion. According to the physics of the transport processes, immediately after the temperature at the left-hand wall is raised to a higher level at $\tau = 0$, the fluid in the cavity adjacent to the wall is driven vertically upward due to the presence of the temperature gradient. This ascending fluid collides with the top wall and is deflected. A weakly recirculating cell is then formed near the wall. It is also observed that the fluid, driven by the small concentration gradient, close to the right-hand wall moves slowly downward. This slow-descending fluid eventually hits the bottom wall and is found to turn left and move along the wall. The flow field for $\tau = 0.90$ in Fig. 1(a) clearly illustrates this phenomenon. At later times, the flow in the enclosure is strengthened by the action of the com-

bined buoyancy forces. The up-moving flow, which is now at higher momentum, in the hydrodynamic boundary layer along the left-hand wall convects the cell downstream toward the top surface through the viscous shearing effects (see the plot for $\tau = 2.73$ in Fig. 1(a)). By and large, the flow is still unit-cellular. As the flow is further accelerated by the buoyancy forces at larger τ, secondary cells appear in the core region ($\tau = 12.33$). Finally, steady state is reached and the flow pattern resembles that without considering the species transfer [25]. Heat and mass transfer in the flow, according to Figs. 1(b) and (c), are respectively conduction and diffusion dominant at the initial transient ($\tau < 0.90$). At later times ($\tau = 2.73$) convection effects set in causing the distortion of the temperature and concentration contours. The thermal and solutal fields finally become boundary-layer type. Because the Prandtl and Schmidt numbers are comparable, the temperature and concentration distributions are analogous.

Next, we investigate the case in which the buoyancy forces are of equal strength. Figures 2(a)–(c) illustrate the transient developments of flow, heat and mass transfer for $Gr = 10^5$ and $N = -1$. In the beginning of the transient ($\tau = 0.24$) two weakly recirculating but counter-rotating cells shown in Fig. 2(a) are almost symmetrically formed close to the vertical walls, which are the consequences of the upward thermal and downward solutal buoyancy forces due to the existence of the temperature and concentration gradients near these walls. It is also noted that the interfacial velocity at the right-hand wall is not negligible because the concentration gradient near it is high at this early transient. These cells grow with time and are carried downstream by the high velocity fluids near the vertical walls (see the figure for $\tau = 2.74$). Meanwhile, the fluids deflected by the top and bottom walls, being at higher velocities, are now capable of crossing the entire enclosure, and thus a primary cell characterized by the high velocity fluid flow along the enclosure walls is noted. The flow then gradually approaches the steady state condition. It is interesting to observe that the flow pattern in this case is again almost the same as that in Fig. 1(a). The time developments of temperature and concentration fields are similar to those for $N = -0.2$ except that the temperature and concentration developments with time become faster and reach almost the same speed.

When the buoyancy ratio is further increased to -5, the flow is expected to be dominated by the solutal buoyancy force. The results shown in Figs. 3(a)–(c) evidently elucidate this point. In contrast to the flow development for $N = -0.2$, a weakly recirculating cell first appears close to the high concentration wall and the fluid flows faster along this wall (plot for $\tau = 0.9$ in Fig. 3(a)). A primary cell is quickly established in the flow along the enclosure walls with two weak cells embedded in it ($\tau = 2.74$). Steady state is gradually approached. It is worth noting that the species transfer is at a higher rate than the energy transfer by comparing the corresponding contour plots in Figs. 3(b) and (c).

According to the results presented in Figs. 1–3, for a given Grashof number steady state is easier to establish when the two driving forces are of approximately equal strength, that is, when the magnitude of N is close to unity. Moreover, it is found that heat transfer is at a faster rate in the flow for $|N| < 1$, while for $|N| > 1$ mass transfer is more effective. Heat and mass transfer is at almost the same rate for $|N| = 1$. The flow patterns in the steady state for the three cases just discussed are nearly the same.

For other Grashof numbers the results obtained in the numerical computations for various N indicate that the influences of the buoyancy ratio on the transient evolution of the flow, temperature and concentration fields are similar to those for $Gr = 10^5$.

4.2. *Opposing flows*

The flow, which is initially at rest, isothermal at T_C and isosolutal at w_{1L}, in the enclosure is now simultaneously driven by the higher temperature and concentration maintained at the left-hand wall. The resulting thermal buoyancy force causes the flow near the left wall to move upward, but the solutal buoyancy force due to the horizontal concentration gradients tends to push the flow downward. As a result, the flow next to the hot wall can move either upward or downward depending on the magnitude of the buoyancy ratio. Again, particular attention is paid herein to the influences of the buoyancy ratio and Grashof number on the transient evolution of the flow field and the associated heat and mass transfer in the enclosure.

As the solutal buoyancy force is small compared with the thermal buoyancy force for $|N| < 1$, in the beginning of the transient the flow near the hot surface is driven vertically upward and a weakly recirculating cell is formed. The results presented in Figs. 4(a)–(c) for $Gr = 10^5$ and $N = -0.2$ apparently confirm this statement. The presence of the small concentration gradients in the flow only slows down but does not reverse the flow. The flow, under the continuing action of the buoyancy forces, speeds up and the cell grows in size (plot for $\tau = 2.74$ in Fig. 4(a)). This growing cell gradually becomes the primary cell moving along the enclosure walls. Secondary cells appear in the core region at later time, and the flow gradually approaches the steady state. That less-effective heat and mass transfer is present in the flow, as noted in Figs. 4(b) and (c), is the result of the slower flow caused by the opposing solutal buoyancy force.

For $|N| > 1$ the solutal buoyancy force, acting downward, overcomes the thermal buoyancy force thereby resulting in a downward flow for the fluid adjacent to the hot wall. This is observed in the results given in Figs. 5(a)–(c) for $Gr = 10^5$ and $N = -5$. Here the thermal buoyancy force, in turn, acts to slow the flow down. The weakly recirculating cell appearing in the initial transient quickly grows in size as time elapses, and the cell gradually evolves into a primary

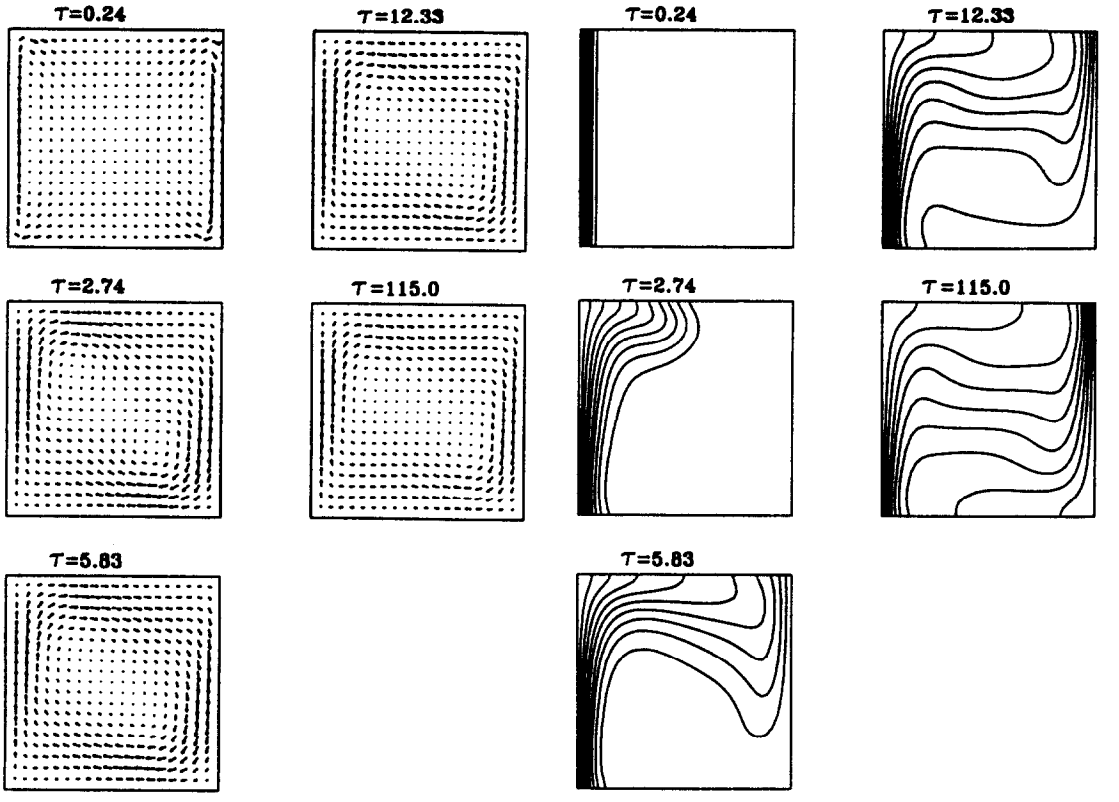

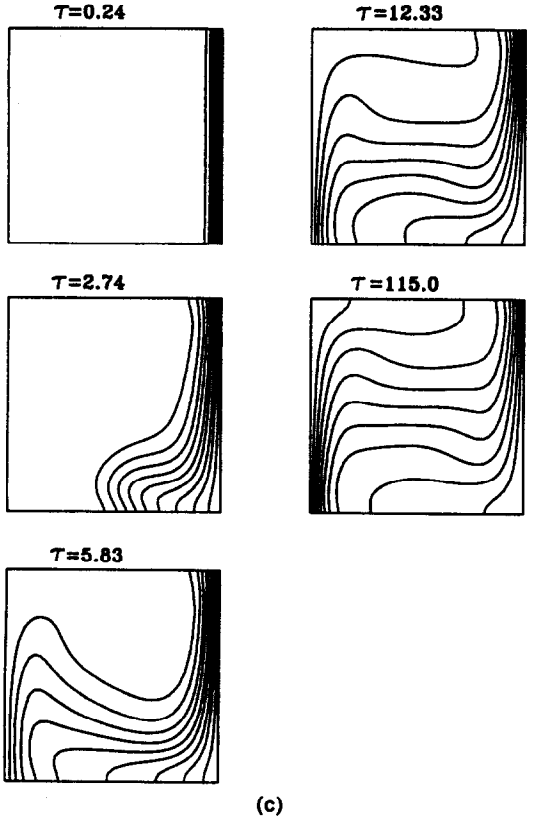

FIG. 2. Time evolution of (a) flow patterns, (b) isotherms and (c) iso-concentration lines in aiding flow for $Gr = 10^5$, $Pr = 0.7$, $Sc = 0.6$, $N = -1$.

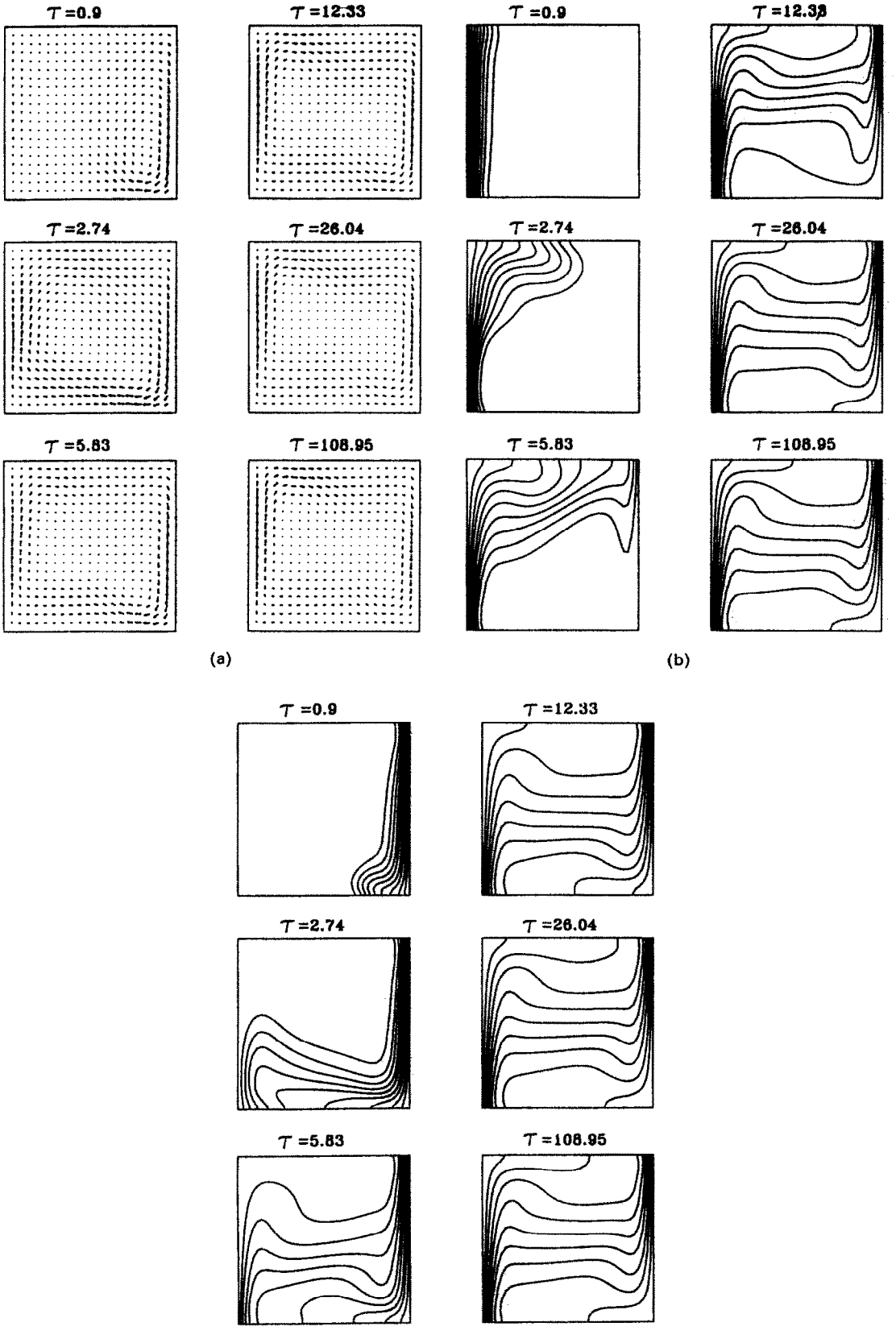

FIG. 3. Time evolution of (a) flow patterns, (b) isotherms and (c) iso-concentration lines in aiding flow for $Gr = 10^5$, $Pr = 0.7$, $Sc = 0.6$, $N = -5$.

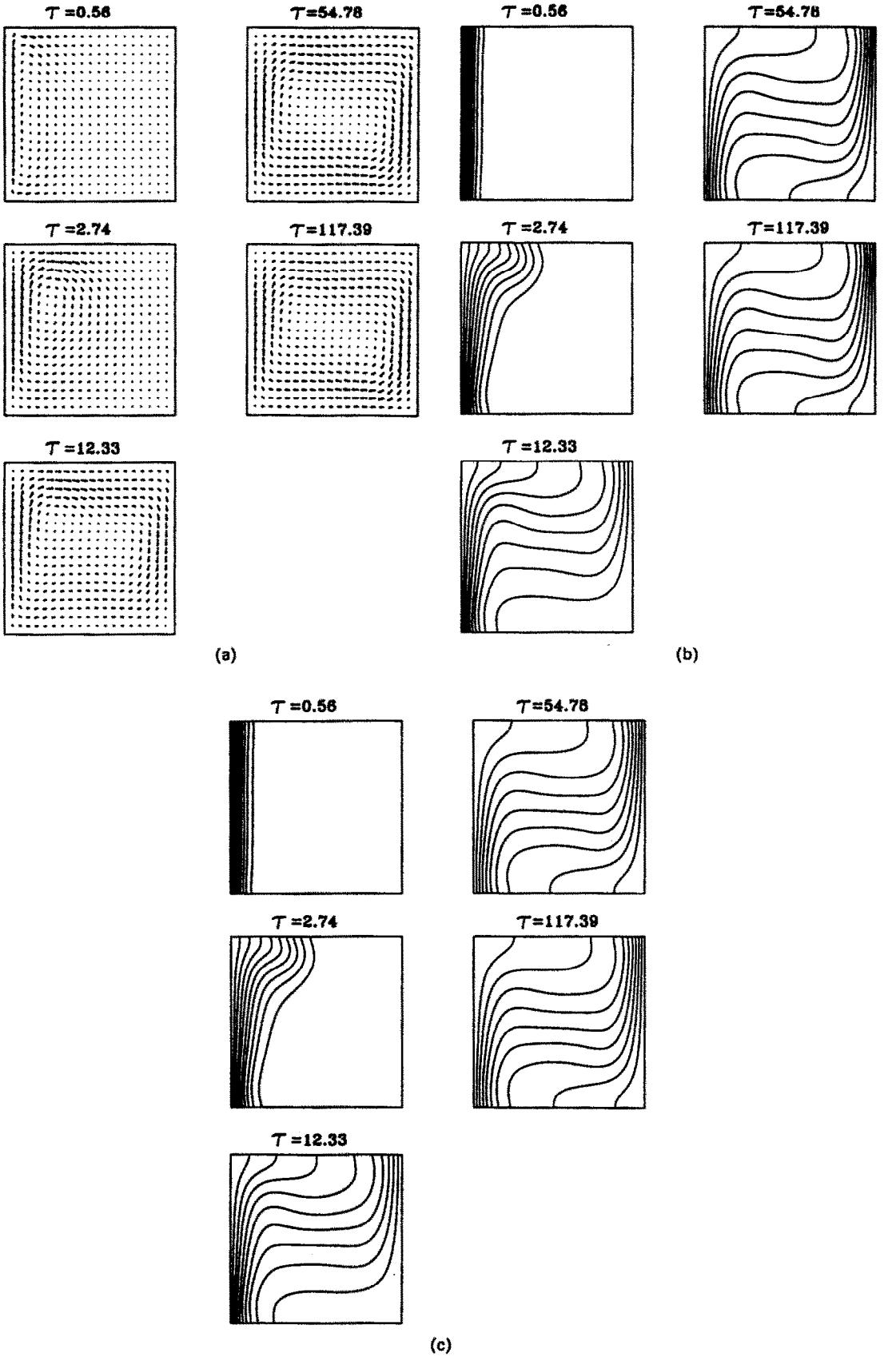

FIG. 4. Time evolution of (a) flow patterns, (b) isotherms and (c) iso-concentration lines in opposing flow for $Gr = 10^5$, $Pr = 0.7$, $Sc = 0.6$, $N = -0.2$.

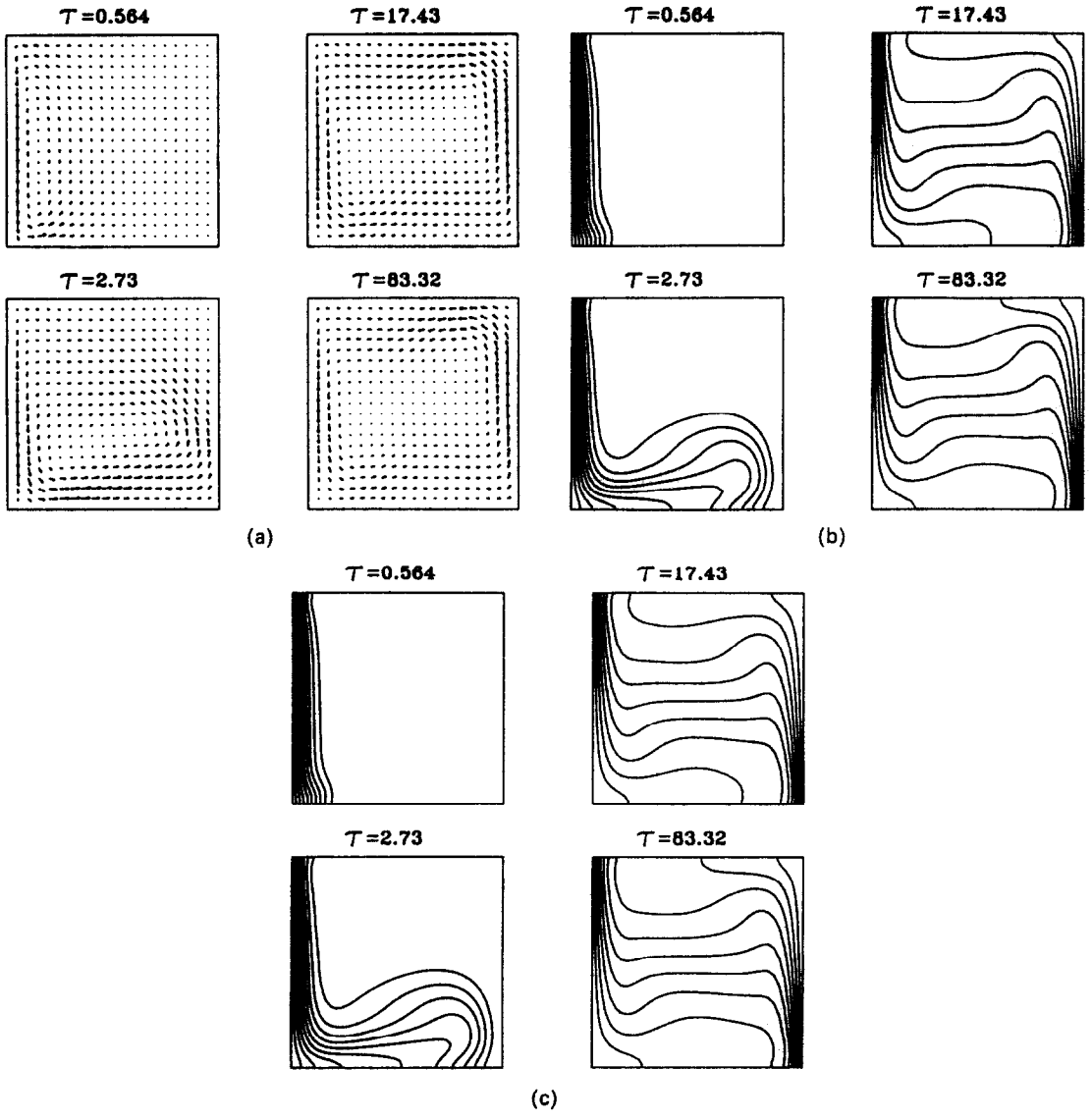

FIG. 5. Time evolution of (a) flow patterns, (b) isotherms and (c) iso-concentration lines in opposing flow for $Gr = 10^5$, $Pr = 0.7$, $Sc = 0.6$, $N = -5$.

cell, moving counterclockwise. Two small, secondary cells are found in the core region at a later time. The flow reaches steady state in a short period of time.

On inspecting the temperature and concentration contours shown in Figs. 4(b), 4(c), 5(b) and 5(c) for opposing flows, it is interesting to notice that as τ exceeds a certain value, the hot and heavy fluid is on the top over the cold and light fluid for the case with $N = -0.2$; the reverse is true for the case with $N = -5$. In the former case the flow is thermally stable but solutally unstable, while the flow is thermally unstable but solutally stable for the later case. Hence, under simultaneous action of the opposing buoyancy forces the flow is prone to become oscillatory during the transient stage, which is similar to the study by Patterson and Imberger [26], Patterson [27] and Briggs and Jones [28] for pure thermal convection.

4.3. *Heat and mass transfer coefficients*

Information on how the presence of species transfer affects natural convection heat and mass transfer coefficients is most relevant to practice. The transient variations of the interfacial velocity and local Nusselt and Sherwood numbers at the left-hand wall at several time instants are shown in Figs. 6–8 for aiding flow with $Gr = 10^5$ and $N = -5$. The results indicate that the interfacial velocity for $\Gamma_1 = 20$ is small compared with the steady U_{max} and V_{max} for pure thermal convection given in Table 1. Obviously, for a smaller Γ_1 the interfacial velocity will exhibit strong effects. At a given X, Fig. 7 indicates that the Nusselt numbers oscillate with time [26–28].

Results presented in Tables 2 and 3 give heat and mass transfer across the enclosure for both aiding and opposing flows at steady state. The results clearly indicate that for aiding flows the average Nusselt num-

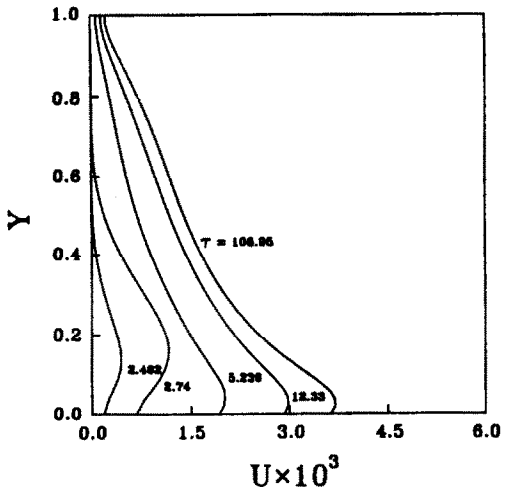

FIG. 6. Transient distributions of the interfacial velocity along the left-hand wall for aiding flow for $Gr = 10^5$, $Pr = 0.7$, $Sc = 0.6$, $N = -5$.

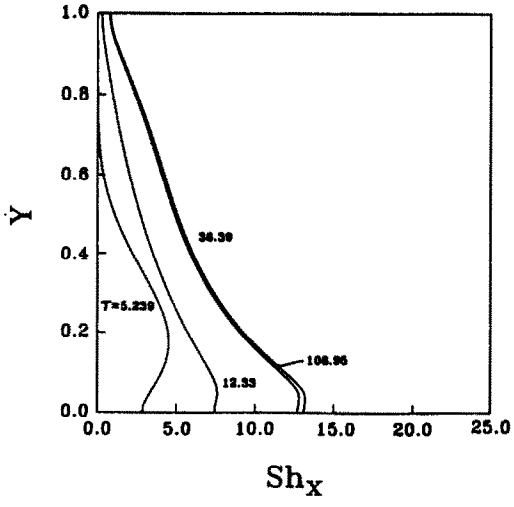

FIG. 8. Transient local Sherwood number distributions along the left-hand wall for aiding flow for $Gr = 10^5$, $Pr = 0.7$, $Sc = 0.6$, $N = -5$.

ber significantly increases when N is raised from -0.2 to -5 for all the Grashof numbers considered. This also holds true for the average Sherwood number. But in the opposing flows the mass transfer effects are much more complex. For $|N| < 1$ the average Nusselt and Sherwood numbers decrease with the magnitude of N. This concurs with the previous discussion that the flow driven by the thermal buoyancy force is weakened by the opposing solutal buoyancy force. When the magnitude of N is much larger than unity, the opposing solutal buoyancy force completely overcomes the thermal buoyancy force, and therefore the flow is more vigorous and heat and mass transfer more effective as the magnitude of the buoyancy ratio is larger. The results for $N = -5$ evidently substantiate this point. Results in Tables 2 and 3 can be correlated by

$$\overline{Nu} = 0.13||N| \pm 1|^{0.23} Gr^{0.3} \quad (19)$$

and

$$\overline{Sh} = 0.12||N| \pm 1|^{0.23} Gr^{0.3} \quad (20)$$

where the '+' and '−' signs are respectively for the aiding and opposing flows. The above correlations are

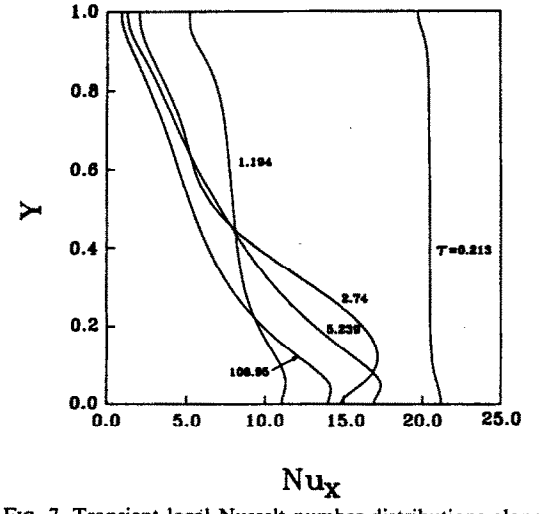

FIG. 7. Transient local Nusselt number distributions along the left-hand wall for aiding flow for $Gr = 10^5$, $Pr = 0.7$, $Sc = 0.6$, $N = -5$.

Table 2. The effects of buoyancy ratio on the average Nusselt number for various Grashof numbers

		Gr		
$\overline{Nu}$	N	10^3	10^5	10^6
	−5	1.6299	6.3250	12.414
aiding	−1	1.2208	5.3487	11.333
	−0.2	1.1170	4.5471	9.821
	0.0	1.0725	4.1556	8.720
	−0.2	1.0294	3.7299	8.028
opposing	−0.9	0.9827	1.5520	2.907
	−5	1.4240	6.0537	10.820

Table 3. The effects of buoyancy ratio on the average Sherwood number for various Grashof numbers

		Gr		
$\overline{Sh}$	N	10^3	10^5	10^6
	−5	1.5183	5.9103	11.463
aiding	−1	1.1698	4.9223	10.375
	−0.2	1.0890	4.1742	8.934
	0.0	1.0480	3.9110	8.135
	−0.2	1.0186	3.4294	7.366
opposing	−0.9	0.9841	1.4306	2.539
	−5	1.3410	5.6417	10.091

not good for the opposing flow with $N = -0.9$ in which two buoyancy forces are almost of equal strength. Interestingly, we noted that $\overline{Sh}/\overline{Nu} = 0.92$ which is equal to $Le^{1/2}$. This outcome is in good agreement with the scale analysis proposed by Bejan [20] for the case with Pr, Sc and Le all smaller than unity.

5. CONCLUDING REMARKS

In this paper transient developments of velocity, temperature and concentration fields in a binary mixture in square enclosures driven by the simultaneous action of thermal and solutal buoyancy forces were numerically investigated. The evolution of the flow pattern and the associated heat and mass transfer were found to be significantly influenced by the buoyancy ratio and the directions of the buoyancy forces. The flow patterns at the steady state, however, resemble each other, irrespective of the buoyancy ratio.

The extension of the present study to natural convection heat and mass transfer in tall and shallow enclosures for various mixtures is of value to many engineering applications. The existence of oscillatory flows in binary systems requires further study. This will be our next task.

Acknowledgement—The support of this study by the National Science Council of Taiwan, R.O.C., is acknowledged.

REFERENCES

1. W. N. Gill, E. D. Casal and D. W. Zeh, Binary diffusion and heat transfer in laminar free convection boundary layers on a vertical plate, *Int. J. Heat Mass Transfer* **8**, 1131–1151 (1965).
2. J. A. Adams and P. W. McFadden, Simultaneous heat and mass transfer in free convection with opposing body forces, *A.I.Ch.E. Jl* **12**, 642–647 (1966).
3. J. W. Taunton, E. N. Lightfoot and W. E. Stewart, Simultaneous free-convection heat and mass transfer in laminar boundary layers, *Chem. Engng Sci.* **25**, 1927–1937 (1970).
4. B. Gebhart and L. Pera, The nature of vertical natural convection flows resulting from the combined buoyancy effects of thermal and mass diffusion, *Int. J. Heat Mass Transfer* **14**, 2025–2050 (1971).
5. F. A. Bottemanne, Theoretical solution of simultaneous heat and mass transfer by free convection about a vertical flat plate, *Appl. Scient. Res.* **25**, 137–149 (1972).
6. G. D. Callahan and W. J. Marner, Transient free convection with mass transfer on an isothermal vertical flat plate, *Int. J. Heat Mass Transfer* **19**, 165–174 (1976).
7. S. Ostrach, Natural convection with combined buoyancy forces, *PCH PhysicoChem. Hydrodyn.* **1**, 233–247 (1980).
8. S. Ostrach, Fluid mechanics in crystal growth—the 1982 Freeman Scholar Lecture, *J. Fluids Engng* **105**, 5–20 (1983).
9. M. Pimputkar and S. Ostrach, Convective effects in crystals grown from melt, *J. Crystal Growth* **55**, 614–646 (1981).
10. W. E. Langlois, Buoyancy-driven flows in crystal-growth melts, *Ann. Rev. Fluid Mech.* **17**, 191–215 (1985).
11. F. Rosenberger, Fluid mechanics in crystal growth from vapors, *PCH PhysicoChem. Hydrodyn.* **1**, 3–26 (1980).
12. B. S. Jhaveri and F. Rosenberger, Expansive convection in vapor transport across horizontal rectangular enclosures, *J. Crystal Growth* **57**, 57–64 (1982).
13. B. L. Markham and F. Rosenberger, Diffusive-convective vapor transport across horizontal and inclined rectangular enclosures, *J. Crystal Growth* **67**, 241–254 (1984).
14. Y. Kamotani, L. W. Wang, S. Ostrach and D. H. Jiang, Experimental study of natural convection in shallow enclosures with horizontal temperature and concentration gradients, *Int. J. Heat Mass Transfer* **28**, 165–173 (1985).
15. S. Ostrach, H. D. Jiang and Y. Kamotani, Thermosolutal convection in shallow enclosures, ASME–JSME Thermal Engng Joint Conf., Hawaii (1987).
16. J. Lee and M. T. Hyun, Experimental study of natural convection due to combined buoyancy in a low-aspect ratio enclosure, ASME–JSME Thermal Engng Joint Conf., Hawaii (1987).
17. L. W. Wang and P. C. Chuang, Flow patterns of natural convection in enclosures with horizontal temperature and concentration gradients, *Proc. 8th Int. Heat Transfer Conf.*, San Francisco, California, Vol. 4, pp. 1477–1481 (1986).
18. P. Ranganathan and R. Viskanta, Natural convection in a binary gas in rectangular cavities, ASME–JSME Thermal Engng Joint Conf., Hawaii (1987).
19. O. V. Trevisan and A. Bejan, Combined heat and mass transfer by natural convection in a vertical enclosure, *J. Heat Transfer* **109**, 104–112 (1987).
20. A. Bejan, Mass and heat transfer by natural convection in a vertical cavity, *Int. J. Heat Fluid Flow* **6**, 149–159 (1985).
21. S. V. Patankar and D. B. Spalding, A calculation procedure for heat, mass and momentum transfer in three-dimensional parabolic flows, *Int. J. Heat Mass Transfer* **15**, 1787–1806 (1972).
22. S. V. Patankar, *Numerical Heat Transfer and Fluid Flow*. Hemisphere/McGraw-Hill, New York (1980).
23. S. V. Patankar, A calculation procedure for two-dimensional elliptic situations, *Numer. Heat Transfer* **4**, 409–425 (1981).
24. F. Rosenberger and G. Muller, Interfacial transport in crystal growth, a parametric comparison of convective effects, *J. Crystal Growth* **65**, 91–104 (1983).
25. G. de Vahl Davis, Natural convection of air in a square cavity: a bench mark numerical solution, *Int. J. Numer. Meth. Fluids* **3**, 249–264 (1983).
26. J. Patterson and J. Imberger, Unsteady natural convection in a rectangular cavity, *J. Fluid Mech.* **100**, 65–86 (1980).
27. J. C. Patterson, On the existence of an oscillatory approach to steady natural convection in cavities, *J. Heat Transfer* **106**, 104–108 (1984).
28. D. G. Briggs and D. N. Jones, Two-dimensional periodic natural convection in a rectangular enclosure of aspect ratio one, *J. Heat Transfer* **107**, 850–854 (1985).

CONVECTION NATURELLE VARIABLE DE MELANGE BINAIRE DANS DES CAVITES CARREES

Résumé—On traite numériquement en détail la convection naturelle variable d'un mélange binaire dans des cavités carrées avec présence simultanée de gradients de température et de concentration. Des résultats sont présentés pour illustrer les effets combinés des forces de flottement thermiques et solutales sur l'évolution temporelle de la configuration de l'écoulement et sur les transferts combinés de chaleur et de masse dans le cas des écoulements favorables ou en opposition. Les effets du rapport de flottement sont particulièrement significatifs vis-à-vis de la configuration de l'écoulement et du transfert de chaleur et de masse dans le cas des écoulements en opposition.

INSTATIONÄRE NATÜRLICHE KONVEKTION EINES BINÄREN GEMISCHES IN QUADRATISCHEN HOHLRÄUMEN

Zusammenfassung—Die instationäre natürliche Konvektion eines binären Gemisches in quadratischen Hohlräumen wird unter dem gleichzeitigen Einfluß von Temperatur- und Konzentrationsgradienten ausführlich numerisch untersucht. Insbesondere werden Ergebnisse dargestellt, die den Einfluß beider Auftriebskräfte auf die zeitliche Entwicklung der Strömungsform und der damit verbundenen Wärme- und Stoffübertragung sowohl für gleichgerichtete als auch für entgegengerichtete Auftriebskräfte zeigen. Es hat sich gezeigt, daß der Einfluß des Verhältnisses der Auftriebskräfte auf die Strömungsform und die Wärme- und Stoffübertragung ziemlich bedeutsam ist, besonders für entgegengerichtete Auftriebskräfte.

НЕУСТАНОВИВШАЯСЯ ЕСТЕСТВЕННАЯ КОНВЕКЦИЯ БИНАРНОЙ СМЕСИ В ПОЛОСТЯХ КВАДРАТНОГО СЕЧЕНИЯ

Аннотация—Выполнено подробное численное исследование неустановившейся естественной конвекции бинарной смеси в полостях квадратного сечения при одновременном воздействии температурного и концентрационного градиентов. В частности, приведены результаты, иллюстрирующие совместное влияние термической и концентрационной выталкивающих сил на временную эволюцию потока и соответствующих процессов тепло- и массопереноса как для однонаправленных, так и для встречных течений. Обнаружено, что картина течения и процессы тепло- и массопереноса довольно существенно зависят от величины отношения подъемных сил, особенно в случае встречных потоков.